FREQUENCY-SELECTIVE HYBRID BEAMFORMING FOR MMWAVE FULL-DUPLEX

Andrea Guamo-Morocho *Roberto López-Valcarce*

atlanTTic Research Center, University of Vigo, Spain. Email: {aguamo,valcarce}@gts.uvigo.es

ABSTRACT

We study beamforming cancellation for a full-duplex (FD) wideband millimeter wave (mmWave) point-to-point bidirectional link in which both multicarrier-based nodes transmit and receive simultaneously and on the same frequency. The focus is on hybrid architectures in which the analog subblock of the beamformer, common to all subcarriers, is fully-connected and based on phase shifters with finite resolution, to avoid frontend saturation by mitigating FD-induced self-interference in the analog domain.

***Index Terms*—** Wideband mmWave, hybrid beamforming, full-duplex, multicarrier modulation, self-interference.

1. INTRODUCTION

Future high data rate systems envisage multi-input multi-output (MIMO) communication at millimeter wave (mmWave) frequencies due to the availability of wide bandwidths [1, 2], using large antenna arrays to overcome large propagation losses at such frequencies. Fully digital beamforming is not suitable due to the high cost and power consumption of having a dedicated radio frequency (RF) chain per antenna, so hybrid solutions, splitting the processing between the digital baseband and analog RF domains, have been proposed as a means to reduce the number of RF chains [3, 4]. Application to mmWave communication of in-band full-duplex (FD), *i.e.,* simultaneous transmission (TX) and reception (RX) in the same frequency, is attracting interest [5–7] because of its potential to double spectral efficiency and to add flexibility to multiple access schemes and point-to-point handshaking [8].

The main obstacle to FD is *self-interference* (SI) produced by an FD node's own transmission, as it will leak to its own receiver, overwhelming the much weaker signals of interest from remote transmitters. Recent FD advances for sub-6 GHz systems combine propagation-, analog circuit-, and digital-domain approaches to SI mitigation [9]. Whereas analog circuit-domain methods are essential to avoid RX frontend saturation, they scale poorly with array size, which hampers application to mmWave. At the same time, large arrays offer new opportunities to suppress SI in the spatial domain without additional specialized RF circuitry, via beamforming cancellation (BFC). In the FD mmWave context, a number of BFC designs [10–15] have been proposed under different scenarios and architectures, including all-digital as well as hybrid beamforming structures based on finite-resolution phase shifters (PS). These BFC-based schemes assume frequency-flat channels; yet wideband operation is envisioned for mmWave systems, so it is more realistic to assume that channels will be frequency-selective [16–18]. Whereas orthogonal frequency-division multiplexing (OFDM) can transform the frequency-selective MIMO channel into a set of parallel frequency-flat MIMO subchannels for the different subcarriers, the fact that the RF component of hybrid beamformers is frequency-flat, *i.e.,* common to all subcarriers, introduces additional design constraints.

A few schemes have been proposed for wideband FD mmWave. Analog circuit-domain and baseband SI cancellation, rather than BFC, are the focus of [19,20]. In [21] BFC is considered, selecting the RF beamformers from some dictionary (*e.g.,* a DFT codebook) via orthogonal matching pursuit to approximate the singular vectors of channel matrices, and then adopting a regularized zero forcing (RZF) design for their baseband counterparts. We present a BFC-based design whose main differences with [21] are as follows. First, we consider a device-to-device network with two FD-capable nodes, whereas in [21] an FD node transmits to and receives from two half-duplex (HD) nodes. Second, using DFT codebooks for the RF beamformers requires at least $\log_2 N$-bit PS resolution, with N the array size; this may be troublesome for large arrays. We allow for arbitrary PS resolution, independent of array size. Third, [21] targets SI mitigation at the baseband combiner output, which could be too late as A/D converters may have already saturated; whereas we specifically aim at reducing SI before A/D conversion.

2. SYSTEM MODEL

Consider a two-node mmWave MIMO-OFDM network using K subcarriers, where both nodes have FD capabilities and separate TX-RX arrays. The TX at node $i \in \{1, 2\}$, equipped with $L_{t,i}$ RF chains and $N_{t,i}$ antennas, sends $N_{s,i}$ data streams over the mmWave channel to the RX of node $j \in \{1, 2\}$, $j \neq i$, equipped with $N_{r,j}$ antennas and $L_{r,j}$ RF chains. Thus, $N_{s,i} \leq L_{t,i} \leq N_{t,i}$ and $N_{s,i} \leq L_{r,j} \leq N_{r,j}$. Vectors $\boldsymbol{s}_i[k] \in \mathbb{C}^{N_{s,i}}$, transmitted by node i at subcarrier

This work was funded by MCIN/ AEI/10.13039/501100011033/ FEDER "Una manera de hacer Europa" under project RODIN (PID2019-105717RB-C21) and fellowship PRE2020-096625.

$k \in \{0, 1, \ldots, K-1\}$, are independent across subcarriers and zero-mean, with covariance $\mathbb{E}\{\boldsymbol{s}_i[k]\boldsymbol{s}_i^H[k]\} = \frac{1}{KN_{s,i}}\boldsymbol{I}_{N_{s,i}}$. A hybrid precoder $\boldsymbol{F}_i[k] = \boldsymbol{F}_{\mathrm{RF},i}\boldsymbol{F}_{\mathrm{BB},i}[k] \in \mathbb{C}^{N_{t,i}\times N_{s,i}}$ is assumed, with $\boldsymbol{F}_{\mathrm{RF},i} \in \mathbb{C}^{N_{t,i}\times L_{t,i}}$ the analog precoder, shared by all subcarriers, and $\boldsymbol{F}_{\mathrm{BB},i}[k] \in \mathbb{C}^{L_{t,i}\times N_{s,i}}$ the digital precoder for subcarrier k. Node i applies $L_{t,i}$ parallel K-point IFFTs to the baseband-precoded vectors $\boldsymbol{F}_{\mathrm{BB},i}[k]\boldsymbol{s}_i[k]$ and adds a cyclic prefix (CP) to each of the $L_{t,i}$ time-domain sequences, which are then upconverted, applied to the RF precoder $\boldsymbol{F}_{\mathrm{RF},i}$ and fed to the $N_{t,i}$ antennas. We adopt the clustered model [16] for the T_s-sampled impulse response of the wideband mmWave MIMO $i \to j$ channel, $i \neq j$:

$$\mathsf{H}_{ij}[d] = \sum_{c=1}^{C}\sum_{r=1}^{R_c} \alpha_{c,r}^{(ij)} p(dT_s - \tau_{c,r}^{(ij)})\boldsymbol{a}_{\mathrm{R},j}(\phi_{c,r}^{(ij)})\boldsymbol{a}_{\mathrm{T},i}^H(\theta_{c,r}^{(ij)}), \tag{1}$$

with C and R_c the total number of clusters and rays per cluster, resp.; $\alpha_{c,r}^{(ij)}$, $\tau_{c,r}^{(ij)}$, $\phi_{c,r}^{(ij)}$ and $\theta_{c,r}^{(ij)}$ the complex gain, time delay, angle of arrival (AoA), and of departure (AoD) of the (c, r) path; $\boldsymbol{a}_{\mathrm{T},i}(\theta)$, $\boldsymbol{a}_{\mathrm{R},j}(\phi)$, the transmit and receive array steering vectors; and $p(t)$ the shaping pulse. The maximum delay D is assumed no larger than the CP length, so that the frequency-domain channel matrix at subcarrier k is given by

$$\boldsymbol{H}_{ij}[k] = \sum_{d=0}^{D} \mathsf{H}_{ij}[d]e^{-j\frac{2\pi k}{K}d}, \quad k = 0, 1, \ldots, K-1. \tag{2}$$

SI channels consist of (i) a line-of-sight (LOS), near-field component $\mathsf{H}_{ii}^{\mathrm{LOS}}$ [5, 12, 21]; (ii) a non-LOS (NLOS) term due to nearby scatterers and denoted $\mathsf{H}_{ii}^{\mathrm{NLOS}}[d]$, following the same model as (1). If $r_{pq}^{(ii)}$ is the distance from element p of the TX array to element q of the RX array of node i, and λ the wavelength, then $[\mathsf{H}_{ii}^{\mathrm{LOS}}]_{pq} = \frac{1}{r_{pq}^{(ii)}}\exp(-j\frac{2\pi}{\lambda}r_{pq}^{(ii)})$. Thus,

$$\mathsf{H}_{ii}[d] = \sqrt{\frac{\kappa}{\kappa+1}}\mathsf{H}_{ii}^{\mathrm{LOS}}\delta[d] + \sqrt{\frac{1}{\kappa+1}}\mathsf{H}_{ii}^{\mathrm{NLOS}}[d], \tag{3}$$

with κ the Rician factor. Note that, following [21], the LOS component in (3) is assumed frequency-flat[1]. Analogously to (2), the frequency-domain SI channel matrices $\boldsymbol{H}_{ii}[k]$ are obtained as the DFT of (3). Frequency-domain channel matrices are assumed normalized so that $\frac{1}{K}\sum_{k=0}^{K-1}\|\boldsymbol{H}_{ij}[k]\|_F^2 = N_{t,i}N_{r,j}\ \forall i, j \in \{1, 2\}$.

The RX of node $j \neq i$ applies a linear combiner $\boldsymbol{W}_j[k] \in \mathbb{C}^{N_{r,j}\times N_{s,i}}$ at subcarrier k. Under perfect synchronization, after CP removal and FFT processing, the received signal is

$$\boldsymbol{y}_j[k] = \underbrace{\sqrt{\rho_i}\boldsymbol{W}_j^H[k]\boldsymbol{H}_{ij}[k]\boldsymbol{F}_i[k]\boldsymbol{s}_i[k]}_{\text{desired signal}} + \underbrace{\sqrt{\eta_j}\boldsymbol{W}_j^H[k]\boldsymbol{H}_{jj}[k]\boldsymbol{F}_j[k]\boldsymbol{z}_j[k] + \boldsymbol{W}_j^H[k]\boldsymbol{n}_j[k]}_{\text{SI+noise}}, \tag{4}$$

where $\boldsymbol{n}_j[k] \sim \mathcal{CN}(\boldsymbol{0}, \sigma_j^2\boldsymbol{I}_{N_{r,j}})$ is the additive noise, and $\boldsymbol{z}_j[k]$, collecting all SI left over after any previous SI mitigation stages that may be present (*i.e.,* at the propagation and analog circuit domains), is assumed zero-mean with covariance $\frac{1}{KN_{s,j}}\boldsymbol{I}_{N_{s,j}}$. Note that in general $\boldsymbol{z}_j[k]$ will be different from $\boldsymbol{s}_j[k]$, because of the distortion introduced by hardware imperfections in the RF frontends. Thus, we regard $\boldsymbol{z}_j[k]$ as unknown and random. In (4), ρ_i and η_j respectively quantify the strength of the desired and SI components.

Hybrid combiners $\boldsymbol{W}_j[k] = \boldsymbol{W}_{\mathrm{RF},j}\boldsymbol{W}_{\mathrm{BB},j}[k]$ are assumed, with $\boldsymbol{W}_{\mathrm{RF},j} \in \mathbb{C}^{N_{r,j}\times L_{r,j}}$ the analog term (common to all subcarriers) and $\boldsymbol{W}_{\mathrm{BB},j}[k] \in \mathbb{C}^{L_{r,j}\times N_{s,i}}$ the baseband combiners. RF precoders and combiners are implemented as fully-connected, finite-resolution PS-based networks, so that $\boldsymbol{F}_{\mathrm{RF},i} \in \mathbb{V}_{b_{t,i}}^{N_{t,i}\times L_{t,i}}$, $\boldsymbol{W}_{\mathrm{RF},i} \in \mathbb{V}_{b_{r,i}}^{N_{r,i}\times L_{r,i}}$, where $\mathbb{V}_b^{N\times L}$ is the set of $N \times L$ matrices whose entries have unit magnitude, and phases taking values in $\{2\pi\ell/2^b,\ \ell = 0, 1, \ldots, 2^b - 1\}$.

3. PROBLEM STATEMENT

Let $\epsilon_{ij} \triangleq \frac{\rho_i}{K\sigma_j^2}$, $i \neq j$, and $\epsilon_{jj} \triangleq \frac{\eta_j}{K\sigma_j^2}$, respectively denote the signal-to-noise ratio (SNR) and (self-) interference-to-noise ratio (INR) at the receiver of node j, and let $\widetilde{\boldsymbol{H}}_{ij}[k] = \boldsymbol{W}_j^H[k]\boldsymbol{H}_{ij}[k]\boldsymbol{F}_i[k]$. As in previous works [10–15, 21], perfect channel state information is asumed. Then, treating SI as noise, and assuming Gaussian signaling, the spectral efficiency for the $i \to j$ link, $i \neq j$, is

$$\mathcal{R}_{ij} = \frac{1}{K}\sum_{k=0}^{K-1}\log_2\left|\boldsymbol{I}_{N_{s,i}} + \frac{\epsilon_{ij}}{N_{s,i}}\widetilde{\boldsymbol{H}}_{ij}^H[k]\boldsymbol{R}_j^{-1}[k]\widetilde{\boldsymbol{H}}_{ij}[k]\right| \tag{5}$$

with $\boldsymbol{R}_j[k] = \frac{\epsilon_{jj}}{N_{s,j}}\widetilde{\boldsymbol{H}}_{jj}[k]\widetilde{\boldsymbol{H}}_{jj}^H[k] + \boldsymbol{W}_j^H[k]\boldsymbol{W}_j[k]$, so that $\sigma_j^2\boldsymbol{R}_j[k]$ is the SI+noise covariance at node j, subcarrier k. The goal is to maximize $\mathcal{R} = \mathcal{R}_{12} + \mathcal{R}_{21}$, under $\boldsymbol{F}_{\mathrm{RF},i} \in \mathbb{V}_{b_{t,i}}^{N_{t,i}\times L_{t,i}}$, $\boldsymbol{W}_{\mathrm{RF},i} \in \mathbb{V}_{b_{r,i}}^{N_{r,i}\times L_{r,i}}$ and TX power constraints

$$\sum_{k=0}^{K-1}\|\boldsymbol{F}_i[k]\|_F^2 = KN_{s,i}, \quad i \in \{1, 2\}. \tag{6}$$

We shall pursue a suboptimal approach to this challenging non-convex problem. A benchmark upper bound on $\mathcal{R}$ can be obtained by neglecting the constraints imposed by the hybrid structure (thus, assuming all-digital beamforming) and assuming that SI is absent ($\epsilon_{11} = \epsilon_{22} = 0$). In that case the optimal $\boldsymbol{F}_i[k]$ and $\boldsymbol{W}_j[k]$ are obtained from the dominant right and left singular vectors of $\boldsymbol{H}_{ij}[k]$ resp., with power allocation across streams and subcarriers obtained via waterfilling.

4. ALL-DIGITAL DESIGN

As starting point for the hybrid design, consider an all-digital approach. Even regarding $\{\boldsymbol{F}_i[k], \boldsymbol{W}_j[k]\}$ as free parameters, the presence of SI makes the problem intractable. As a suboptimal yet tractable alternative, we adopt per-subcarrier ZF

[1] Acknowledging that the mmWave SI channel has not been well characterized yet, the above model may not be completely realistic; nevertheless, we remark that our design does not exploit its particular structure.

constraints, and maximize $\mathcal{R}$ subject to $\widetilde{\boldsymbol{H}}_{jj}[k]=\boldsymbol{0}$ for all k and j, and the power constraint (6). It can be assumed w.l.o.g. that (i) $\boldsymbol{W}_j[k]$ is semiunitary; (ii) $\boldsymbol{F}_i[k]=\boldsymbol{U}_i[k]\boldsymbol{\Sigma}_i[k]$, with $\boldsymbol{U}_i[k]\in\mathbb{C}^{N_{t,i}\times N_{s,i}}$ semiunitary and $\boldsymbol{\Sigma}_i[k]\in\mathbb{R}^{N_{s,i}\times N_{s,i}}$ diagonal positive semidefinite, with diagonal elements in decreasing order. For semiunitary combiners, and under the ZF constraint, $\boldsymbol{R}_j[k]=\boldsymbol{I}_{N_{s,i}}$ in (5), so the problem becomes

$$\max_{\substack{\{\boldsymbol{\Sigma}_i[k],\,\boldsymbol{U}_i[k],\\ \boldsymbol{W}_i[k]\}}} \frac{1}{K}\sum_{k=0}^{K-1}\sum_{\substack{i,j=1\\ j\neq i}}^{2}\log_2\Big|\boldsymbol{I}_{N_{s,i}}+\frac{\epsilon_{ij}}{N_{s,i}}\boldsymbol{\Sigma}_i^2[k]\boldsymbol{U}_i^H[k] \times\boldsymbol{H}_{ij}^H[k]\boldsymbol{W}_j[k]\boldsymbol{W}_j^H[k]\boldsymbol{H}_{ij}[k]\boldsymbol{U}_i[k]\Big| \quad (7)$$

$$\text{s. to}\begin{cases}\boldsymbol{W}_j^H[k]\boldsymbol{W}_j[k]=\boldsymbol{I}_{N_{s,i}}, & \boldsymbol{W}_i^H[k]\boldsymbol{H}_{ii}[k]\boldsymbol{F}_i[k]=\boldsymbol{0},\\ \boldsymbol{U}_i^H[k]\boldsymbol{U}_i[k] \;\;=\boldsymbol{I}_{N_{s,i}}, & \sum_{k=0}^{K-1}\mathsf{Tr}\boldsymbol{\Sigma}_i^2[k]=KN_{s,i}.\end{cases}$$

The coupling among variables introduced by the ZF constraints preclude a closed-form solution for (7), but it is possible to proceed cyclically by optimizing the combiners assuming fixed precoders, and vice versa, as stated next:

1. Given $\boldsymbol{F}_i[k]=\boldsymbol{U}_i[k]\boldsymbol{\Sigma}_i[k]$, for $j\in\{1,2\}$, $i\neq j$, solve:

$$\max_{\{\boldsymbol{W}_j[k]\}}\frac{1}{K}\sum_{k=0}^{K-1}\log_2\Big|\boldsymbol{I}_{N_{s,i}}+\frac{\epsilon_{ij}}{N_{s,i}}\boldsymbol{W}_j^H[k]\boldsymbol{H}_{ij}[k]\boldsymbol{F}_i[k] \times\boldsymbol{F}_i^H[k]\boldsymbol{H}_{ij}^H[k]\boldsymbol{W}_j[k]\Big| \quad (8)$$

$$\text{s. to}\quad \boldsymbol{W}_j^H[k]\boldsymbol{W}_j[k]=\boldsymbol{I}_{N_{s,i}},\;\; \boldsymbol{W}_j^H[k]\boldsymbol{H}_{jj}[k]\boldsymbol{F}_j[k]=\boldsymbol{0}.$$

2. Given $\boldsymbol{W}_j[k]$, for $i\in\{1,2\}$, $j\neq i$, solve:

$$\max_{\{\boldsymbol{\Sigma}_i[k],\,\boldsymbol{U}_i[k]\}}\frac{1}{K}\sum_{k=0}^{K-1}\log_2\Big|\boldsymbol{I}_{N_{s,i}}+\frac{\epsilon_{ij}}{N_{s,i}}\boldsymbol{\Sigma}_i^2[k]\boldsymbol{U}_i^H[k] \times\boldsymbol{H}_{ij}^H[k]\boldsymbol{W}_j[k]\boldsymbol{W}_j^H[k]\boldsymbol{H}_{ij}[k]\boldsymbol{U}_i[k]\Big| \quad (9)$$

$$\text{s. to}\begin{cases}\boldsymbol{U}_i^H[k]\boldsymbol{H}_{ii}^H[k]\boldsymbol{W}_i[k]=\boldsymbol{0}, & \boldsymbol{U}_i^H[k]\boldsymbol{U}_i[k]=\boldsymbol{I}_{N_{s,i}},\\ \sum_{k=0}^{K-1}\mathsf{Tr}\boldsymbol{\Sigma}_i^2[k]=KN_{s,i}.\end{cases}$$

The two steps above are iterated until convergence. Note that, if the power allocation variables $\{\boldsymbol{\Sigma}_i[k]\}$ are held fixed in (9), the resulting problem is structurally equivalent to (8), and is decoupled across subcarriers. The generic solution is given by the following result (the proof is skipped for lack of space).

Lemma 1. *Let $M\geq N+P$. For given $\boldsymbol{A}\in\mathbb{C}^{M\times N}$, $\boldsymbol{C}\in\mathbb{C}^{M\times P}$, and diagonal $\boldsymbol{D}^2\in\mathbb{R}^{N\times N}$ with nonnegative diagonal elements in descending order, the solution to*

$$\max_{\boldsymbol{X}}\big|\boldsymbol{I}_N+\boldsymbol{D}^2\boldsymbol{X}^H\boldsymbol{A}\boldsymbol{A}^H\boldsymbol{X}\big|\;\; s.\; to\begin{cases}\boldsymbol{X}^H\boldsymbol{X} &= \boldsymbol{I}_N,\\ \boldsymbol{X}^H\boldsymbol{C} &= \boldsymbol{0},\end{cases} \quad (10)$$

does not depend on $\boldsymbol{D}^2$, and is given by the N principal left singular vectors of $\boldsymbol{P}_\perp\boldsymbol{A}$, with $\boldsymbol{P}_\perp\in\mathbb{C}^{M\times M}$ the orthogonal projector onto the subspace orthogonal to the columns of $\boldsymbol{C}$. The attained maximum equals $|\boldsymbol{I}_N+\boldsymbol{D}^2\boldsymbol{S}^2|$, with $\boldsymbol{S}^2$ diagonal with the eigenvalues of $\boldsymbol{A}^H\boldsymbol{P}_\perp\boldsymbol{A}$ in descending order.

$M\geq N+P$ means the number of antennas ($M=N_{r,j}$ or $M=N_{t,i}$) be no less than the sum of dimensions of the signal of interest ($N=N_{s,i}$) and interference ($P=N_{s,j}$). Applying Lemma 1 to (8) with $\boldsymbol{D}^2=\frac{\epsilon_{ij}}{N_{s,i}}\boldsymbol{I}$, $\boldsymbol{A}=\boldsymbol{H}_{ij}[k]\boldsymbol{F}_i[k]$, $\boldsymbol{C}=\boldsymbol{H}_{jj}[k]\boldsymbol{F}_j[k]$ yields the optimal combiners $\{\boldsymbol{W}_j^\star[k]\}$, whereas application to (9) with $\boldsymbol{D}^2=\frac{\epsilon_{ij}}{N_{s,i}}\boldsymbol{\Sigma}_i^2[k]$, $\boldsymbol{A}=\boldsymbol{H}_{ij}^H[k]\boldsymbol{W}_j[k]$, $\boldsymbol{C}=\boldsymbol{H}_{ii}^H[k]\boldsymbol{W}_i[k]$ yields the semiunitary part of the optimal precoders, $\{\boldsymbol{U}_i^\star[k]\}$. To find the optimal power allocation matrices $\{\boldsymbol{\Sigma}_i^\star[k]\}$, let $\boldsymbol{P}_i[k]$ be the orthogonal projector onto the subspace orthogonal to the columns of $\boldsymbol{H}_{ii}^H[k]\boldsymbol{W}_i^\star[k]$, and let $\boldsymbol{S}_i^2[k]$ be diagonal with the eigenvalues (in descending order) of $(\boldsymbol{W}_j^\star[k])^H\boldsymbol{H}_{ij}[k]\boldsymbol{P}_i[k]\boldsymbol{H}_{ij}^H[k]\boldsymbol{W}_j^\star[k]$. The standard water-filling algorithm [22] can be used to solve

$$\max_{\{\boldsymbol{\Sigma}_i[k]\}}\frac{1}{K}\sum_{k=0}^{K-1}\log_2\Big|\boldsymbol{I}_{N_{s,i}}+\frac{\epsilon_{ij}}{N_{s,i}}\boldsymbol{\Sigma}_i^2[k]\boldsymbol{S}_i^2[k]\Big| \quad (11)$$
$$\text{s. to}\quad \sum_{k=0}^{K-1}\mathsf{Tr}\boldsymbol{\Sigma}_i^2[k]=KN_{s,i}.$$

Iteration (8)-(9) is a block-coordinate ascent scheme in which the objective does not decrease at each step and is bounded above; thus, convergence in the objective must take place.

5. HYBRID PRECODER DESIGN

The hybrid precoders are obtained by approximating their all-digital counterparts, found as per Sec. 4, in terms of Euclidean distance. Define $\boldsymbol{F}_i\in\mathbb{C}^{N_{t,i}\times KN_{s,i}}$, $\boldsymbol{F}_{\mathrm{BB},i}\in\mathbb{C}^{L_{t,i}\times KN_{s,i}}$ as

$$\boldsymbol{F}_i\triangleq\big[\;\boldsymbol{F}_i[0]\quad\boldsymbol{F}_i[1]\quad\cdots\quad\boldsymbol{F}_i[K-1]\;\big], \quad (12)$$

$$\boldsymbol{F}_{\mathrm{BB},i}\triangleq\big[\;\boldsymbol{F}_{\mathrm{BB},i}[0]\quad\boldsymbol{F}_{\mathrm{BB},i}[1]\quad\cdots\quad\boldsymbol{F}_{\mathrm{BB},i}[K-1]\;\big]. \quad (13)$$

Then, given $\boldsymbol{F}_i$, the problem becomes

$$\min_{\boldsymbol{F}_{\mathrm{RF},i},\,\boldsymbol{F}_{\mathrm{BB},i}}\|\boldsymbol{F}_i-\boldsymbol{F}_{\mathrm{RF},i}\boldsymbol{F}_{\mathrm{BB},i}\|_F^2 \quad (14)$$
$$\text{s. to}\quad \boldsymbol{F}_{\mathrm{RF},i}\in\mathbb{V}_{b_{t,i}}^{N_{t,i}\times L_{t,i}}\;,\;\|\boldsymbol{F}_{\mathrm{RF},i}\boldsymbol{F}_{\mathrm{BB},i}\|_F^2=KN_{s,i}.$$

The first constraint makes problem (14) quite challenging, so we propose a cyclic approach as follows:

1. Given $\boldsymbol{F}_i$ and the RF precoder $\boldsymbol{F}_{\mathrm{RF},i}$, solve

$$\min_{\boldsymbol{F}_{\mathrm{BB},i}}\|\boldsymbol{F}_i-\boldsymbol{F}_{\mathrm{RF},i}\boldsymbol{F}_{\mathrm{BB},i}\|_F^2\;\;\text{s. to}\;\;\|\boldsymbol{F}_{\mathrm{RF},i}\boldsymbol{F}_{\mathrm{BB},i}\|_F^2=KN_{s,i}. \quad (15)$$

The solution to (15) is $\boldsymbol{F}_{\mathrm{BB},i}=c\overline{\boldsymbol{F}}_{\mathrm{BB},i}$, where $\overline{\boldsymbol{F}}_{\mathrm{BB},i}=(\boldsymbol{F}_{\mathrm{RF},i}^H\boldsymbol{F}_{\mathrm{RF},i})^{-1}\boldsymbol{F}_{\mathrm{RF},i}^H\boldsymbol{F}_i$ is the Least Squares solution, and $c=\sqrt{KN_{s,i}}/\|\boldsymbol{F}_{\mathrm{RF},i}\overline{\boldsymbol{F}}_{\mathrm{BB},i}\|_F$ is a normalization constant.

2. Given $\boldsymbol{F}_i$ and the baseband precoder $\boldsymbol{F}_{\mathrm{BB},i}$, solve

$$\min_{\boldsymbol{F}_{\mathrm{RF},i}}\|\boldsymbol{F}_i-\boldsymbol{F}_{\mathrm{RF},i}\boldsymbol{F}_{\mathrm{BB},i}\|_F^2\;\;\text{s. to}\;\;\boldsymbol{F}_{\mathrm{RF},i}\in\mathbb{V}_{b_{t,i}}^{N_{t,i}\times L_{t,i}}. \quad (16)$$

The power constraint is neglected in (16), since it is already taken care of in Step 1. Subproblem (16) has no closed-form solution; it can be approached by cyclically optimizing w.r.t. one of the entries of $\boldsymbol{F}_{\mathrm{RF},i}$ over $\mathbb{V}_{b_{t,i}}^{1\times 1}$ while keeping the remaining entries fixed [17, Sec. IV-B], which can be done in closed form.

The two steps above are iterated until convergence. For initialization, the truncated SVD of $\boldsymbol{F}_i$ (which yields the solution to (14) if the power and hardware constraints are neglected) can be used, by taking $\boldsymbol{F}_{\mathrm{RF},i}$ as the projection onto $\mathbb{V}_b^{N_{t,i}\times L_{t,i}}$ of the $L_{t,i}$ principal left singular vectors of $\boldsymbol{F}_i$.

6. HYBRID COMBINER DESIGN

Note that it is essential to mitigate SI before A/D conversion to avoid converter saturation, and that the RF combiner is common to all subcarriers. Hence, the approach from Sec. 5 to obtain the hybrid precoders by approximating the all-digital ones is not suitable for the combiners, since approximation errors would result in significant SI leakage. Thus, we design the RF combiner by minimizing the SI power at its output, summed over all subcarriers. Let $\boldsymbol{B}_j[k] = \boldsymbol{H}_{jj}[k]\boldsymbol{F}_{\mathrm{RF},j}\boldsymbol{F}_{\mathrm{BB},j}[k]$, where the hybrid precoder has been obtained as per Sec. 5. Then the goal is to minimize $\sum_{k=0}^{K-1}\|\boldsymbol{W}_{\mathrm{RF},j}^H\boldsymbol{B}_j[k]\|_F^2$ subject to $\boldsymbol{W}_{\mathrm{RF},j} \in \mathbb{V}_b^{N_{r,j}\times L_{r,j}}$. Again, this can be approached by cyclically minimizing over each entry of $\boldsymbol{W}_{\mathrm{RF},j}$ while keeping all the others fixed.

Having found $\boldsymbol{W}_{\mathrm{RF},j}$, it remains to obtain the baseband combiners $\boldsymbol{W}_{\mathrm{BB},j}[k]$. These provide additional means to either further mitigate SI at their outputs, or to beamform toward the intended signal. This can be done following the approach from the narrowband design [15] for each subcarrier, which allows to tune the so-called *constraint dimension* d_j to trade off the two objectives above. In the wideband case, one can set the constraint dimension for each subcarrier, so that if $d_j[k] = L_{r,j} - N_{s,j}$ then, at subcarrier k, all the effort is devoted to SI minimization, whereas $d_j[k] = L_{r,j}$ completely focuses on beamforming. See [15, Sec. IV-B] for details.

7. NUMERICAL EXAMPLE

Consider a 50-GHz setting with 200-MHz bandwidth, using 64-element $\frac{\lambda}{2}$-uniform linear arrays. The relative position of TX and RX arrays is as in [15, Fig. 2] with $\alpha = \beta = \frac{\pi}{2}$ and $\delta = 2\lambda$. The number of active subcarriers is $K = 400$, with $1/4$ CP redundancy ($D = 100$), and raised cosine pulse $p(t)$ with 100% roll-off. For NLOS channel terms, 6 clusters and 5 rays per cluster are assumed. The AoA/AoD of each cluster are Gaussian, with random means uniformly distributed in $[0, \pi]$ and standard deviation 16°. Path delays are uniformly distributed in $[0, DT_s]$, whereas path gains are i.i.d. complex circular Gaussian. The Rician factor of SI channels is $\kappa = 10$ dB. Results were averaged over 100 channel realizations.

Transceivers have $N_{t,i} = N_{r,i} = 64$ antennas and $L_{t,i} = L_{r,i} = 8$ RF chains, $i \in \{1, 2\}$, and the number of streams is $N_{s,1} = N_{s,2} = 4$. PS resolution is assumed to be the same for all RF beamformers. In the design of baseband combiners, the constraint dimension is set to 5 for all subcarriers (the admissible range is $\{4, 5, \ldots, 8\}$). Fig. 1 shows the spectral efficiency $\mathcal{R}$ of the proposed FD design as a function of the SNR $\epsilon_{12} = \epsilon_{21}$, assumed to be equal at both nodes, and for INR values $\epsilon_{11} = \epsilon_{22} = 30$ dB. For comparison, we also show the results for an HD system in the same setting[2].

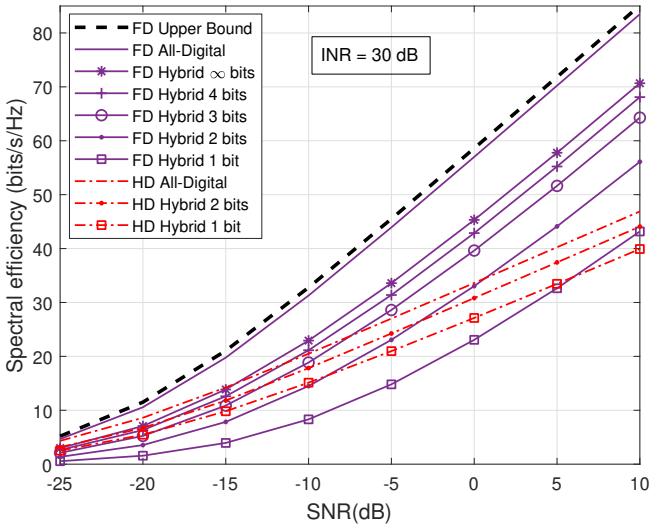

Fig. 1. Spectral efficiency vs. SNR. INR $= 30$ dB.

The all-digital FD design of Sec. 4 performs very close to the SI-free upper bound from Sec. 3, significantly outperforming the all-digital HD design. Hybrid schemes incur a performance loss, which is much more significant for FD than for HD due to the effect of SI leakage. With 1-, 2- and 3-bit PS quantization, FD performs better than HD for SNR larger than 5, -3 and -8 dB, respectively. For 4-bit PS, the FD spectral efficiency is already close to that of an FD system with no PS quantization. The large gap between the latter and the all-digital FD design is due to the constant magnitude constraint on the RF block of hybrid beamformers.

8. CONCLUSION

Under FD operation, the practical constraints applying to hybrid beamformers for wideband mmWave MIMO-OFDM systems make their design challenging. Whereas quasi-optimal beamforming cancellation of SI can be achieved with all-digital structures, for practical phase-shifter resolutions the hybrid architecture presents a significant loss due to SI leakage. Nevertheless, the proposed design still outperforms HD alternatives for sufficiently large SNR. Future work will focus on bridging the performance gap between FD all-digital and hybrid approaches.

[2]The HD all-digital beamformers are obtained from the channel singular vectors, with power allocated via waterfilling. The HD hybrid beamformers are obtained by approximating their all-digital counterparts in terms of Euclidean distance, analogously to the process in Sec. 5.

9. REFERENCES

[1] S. Rangan, T. S. Rappaport, and E. Erkip, "Millimeter wave cellular wireless networks: Potentials and challenges," *Proc. IEEE*, vol. 102, no. 3, pp. 366–385, Mar. 2014.

[2] 3GPP, "TS 38.211: NR; Physical channels and modulation (Release 15)," https://portal.3gpp.org/desktopmodules/Specifications/SpecificationDetails.aspx?specificationId=3213, Mar. 2018.

[3] O. El Ayach, S. Rajagopal, S. Abu-Surra, Z. Pi, and J. R. W. Heath, "Spatially sparse precoding in mmWave MIMO systems," *IEEE Trans. Wireless Commun.*, vol. 13, no. 3, pp. 1499–1513, Mar. 2014.

[4] R. W. Heath, N. González-Prelcic, S. Rangan, W. Roh, and A. Sayeed, "An overview of signal processing techniques for millimeter wave MIMO systems," *IEEE J. Sel. Topics Signal Process.*, vol. 10, no. 3, pp. 436–453, Apr. 2016.

[5] Z. Xiao, P. Xia, and X. G. Xia, "Full-duplex millimeter-wave communication," *IEEE Wireless Commun.*, vol. 24, no. 6, pp. 136–143, 2017.

[6] J. Zhang, N. Garg, M. Holm, and T. Ratnarajah, "Design of full-duplex millimeter-wave integrated access and backhaul networks," *IEEE Wireless Commun.*, vol. 28, no. 1, pp. 60–67, Feb. 2021.

[7] I. P. Roberts, J. G. Andrews, H. B. Jain, and S. Vishwanath, "Millimeter-wave full-duplex radios: New challenges and techniques," *IEEE Wireless Commun.*, vol. 28, no. 1, pp. 36–43, Feb. 2021.

[8] A. Sabharwal, P. Schniter, D. Guo, D. Bliss, S. Rangarajan, and R. Wichman, "In-band full-duplex wireless: Challenges and opportunities," *IEEE J. Sel. Areas Commun.*, vol. 32, no. 9, pp. 1637–1652, Sep. 2014.

[9] K. E. Kolodziej (ed.), *In-band full-duplex wireless systems handbook*. Norwood, MA, USA: Artech House, 2021.

[10] X. Liu, Z. Xiao, L. Bai, J. Choi, P. Xia, and X. G. Xia, "Beamforming based full-duplex for millimeter-wave communication," *Sensors*, vol. 16, no. 7, p. 1130, 2016.

[11] R. López-Valcarce and N. González-Prelcic, "Analog beamforming for full-duplex millimeter wave communication," in *Proc. Int. Symp. Wireless Commun. Syst. (ISWCS)*, 2019, pp. 687–691.

[12] K. Satyanarayana, M. El-Hajjar, P. H. Kuo, A. Mourad, and L. Hanzo, "Hybrid beamforming design for full-duplex millimeter wave communication," *IEEE Trans. Veh. Technol.*, vol. 68, no. 2, pp. 1394–1404, Feb. 2019.

[13] J. M. B. Da Silva, A. Sabharwal, G. Fodor, and C. Fischione, "1-bit phase shifters for large-antenna full-duplex mmWave communications," *IEEE Trans. Wireless Commun.*, vol. 19, no. 10, pp. 6916–6931, Oct. 2020.

[14] I. P. Roberts, J. G. Andrews, and S. Vishwanath, "Hybrid beamforming for millimeter wave full-duplex under limited receive dynamic range," *IEEE Trans. Wireless Commun.*, vol. 20, no. 12, pp. 7758–7772, Dec. 2021.

[15] R. López-Valcarce and M. Martínez-Cotelo, "Full-duplex mmWave MIMO with finite-resolution phase shifters," *IEEE Trans. Wireless Commun.*, vol. 21, no. 11, pp. 8979–8994, Nov. 2022.

[16] A. Alkhateeb and R. W. Heath, "Frequency selective hybrid precoding for limited feedback millimeter wave systems," *IEEE Trans. Commun.*, vol. 64, no. 5, pp. 1801–1818, 2016.

[17] F. Sohrabi and W. Yu, "Hybrid analog and digital beamforming for mmWave OFDM large-scale antenna arrays," *IEEE J. Sel. Areas Commun.*, vol. 35, no. 7, pp. 1432–1443, Jul. 2017.

[18] R. López-Valcarce and N. González-Prelcic, "Hybrid beamforming designs for frequency-selective mmWave MIMO systems with per-RF chain or per-antenna power constraints," *IEEE Trans. Wireless Commun.*, vol. 21, no. 8, pp. 5770–5784, Aug. 2022.

[19] H. Luo, A. Bishnu, and T. Ratnarajah, "On the feasibility and performance of self-interference cancellation in FR2 band," in *Proc. IEEE Int. Conf. Commun. (ICC)*, 2022.

[20] J. Zhang, H. Luo, N. Garg, A. Bishnu, M. Holm, and T. Ratnarajah, "Design and analysis of wideband in-band-full-duplex FR2-IAB networks," *IEEE Trans. Wireless Commun.*, vol. 21, no. 6, pp. 4183–4196, Jun. 2022.

[21] I. P. Roberts, H. B. Jain, and S. Vishwanath, "Frequency-selective beamforming cancellation design for millimeter-wave full-duplex," in *Proc. IEEE Int. Conf. Commun. (ICC)*, 2020.

[22] D. Tse and P. Viswanath, *Fundamentals of wireless communication*. New York, NY, USA: Cambridge University Press, 2005.